

BreastDCEDL: Curating a Comprehensive DCE-MRI Dataset and Developing a Transformer Implementation for Breast Cancer Treatment Response Prediction

Naomi Fridman^{1,*}, Bubby Solway², Tomer Fridman², Itamar Barnea², Anat Goldshtein^{1,†}

¹Ariel University, Israel

²NF Algorithms & AI, Israel

*Corresponding author: naomi.fridman@gmail.com

†Supervisor

Abstract

Breast cancer remains a leading cause of cancer-related mortality worldwide, making early detection and accurate treatment response monitoring critical priorities. We present BreastDCEDL, a curated, deep learning-ready dataset comprising pre-treatment 3D Dynamic Contrast-Enhanced MRI (DCE-MRI) scans from 2,070 breast cancer patients drawn from the I-SPY1, I-SPY2, and Duke cohorts, all sourced from The Cancer Imaging Archive. The raw DICOM imaging data were rigorously converted into standardized 3D NIfTI volumes with preserved signal integrity, accompanied by unified tumor annotations and harmonized clinical metadata including pathologic complete response (pCR), hormone receptor (HR), and HER2 status. Although DCE-MRI provides essential diagnostic information and deep learning offers tremendous potential for analyzing such complex data, progress has been limited by lack of accessible, public, multicenter datasets. BreastDCEDL addresses this gap by enabling development of advanced models, including state-of-the-art transformer architectures that require substantial training data. To demonstrate its capacity for robust modeling, we developed the first transformer-based model for breast DCE-MRI, leveraging Vision Transformer (ViT) architecture trained on RGB-fused images from three contrast phases (pre-contrast, early post-contrast, and late post-contrast). Our ViT model achieved state-of-the-art pCR prediction performance in HR+/HER2⁻ patients (AUC 0.94, accuracy 0.93). BreastDCEDL includes predefined benchmark splits, offering a framework for reproducible research and enabling clinically meaningful modeling in breast cancer imaging.

1 Introduction

Breast cancer remains a leading cause of cancer death worldwide, with early detection and accurate treatment monitoring being crucial for improved patient outcomes. An important clinical decision after diagnosis is the choice between immediate surgery or neoadjuvant chemotherapy (NAC) before surgery. NAC aims to diminish the tumor, enhancing surgical success potential. The optimal outcome is pathologic complete response (pCR)—the absence of residual invasive disease following therapy, confirmed by post-surgical biopsy. Accurate prediction of pCR in the early stage is critical, as it correlates strongly with improved long-term survival and can guide personalized treatment decisions.

Dynamic Contrast-Enhanced MRI (DCE-MRI) serves as a principal imaging modality for breast cancer assessment. The technique involves acquiring sequential 3D scans before and after contrast agent administration, typically analyzed at three timepoints: pre-contrast baseline, early post-contrast (maximum enhancement), and late post-contrast (washout dynamics), as shown in Figure 1. These acquisitions enable visualization of abnormal tumor vascularity—characterized by increased vessel density, permeability, and disorganized structure—that distinguishes malignant tissues from normal breast parenchyma.

The application of deep learning to breast DCE-MRI analysis has demonstrated considerable promise but faces significant limitations. Multiple systematic reviews [7, 8, 23] have identified critical barriers: insufficient accessible large-scale datasets, inconsistent evaluation protocols, and inadequate external validation. While convolutional neural networks have shown promising results through multiphase fusion [15], multimodal integration [4, 11], and multi-institutional validation [2], most investigations remain constrained by limited sample sizes and non-standardized data formats.

Transformer architectures, which have revolutionized natural language processing and computer vision [21], offer substantial potential for medical imaging applications [12]. Their capacity to capture global context makes them particularly suitable for complex volumetric inputs such as DCE-MRI. However, their implementation in breast cancer imaging has been hindered by the absence of sufficiently large, standardized datasets.

To address these challenges, we present BreastDCEDL, the first comprehensive deep learning-ready dataset for breast DCE-MRI. By integrating data from I-SPY-2 [22] (985 patients), Duke [1] (922 patients), and I-SPY-1 [19] (221 patients), we have created a standardized resource of unprecedented scale. The dataset transforms complex DICOM structures into accessible 3D arrays with preserved signal integrity, unified tumor annotations, and harmonized clinical metadata.

Utilizing this resource, we implemented a Vision Transformer (ViT) workflow for DCE-MRI analysis. Our approach demonstrates the feasibility of applying transformer architectures to this complex imaging modality, achieving state-of-the-art performance in pCR prediction. This implementation represents the first successful application of transformer models to breast DCE-MRI data.

Through BreastDCEDL and our transformer-based modeling workflow, we

aim to accelerate progress in AI-assisted breast cancer care by providing the research community with the resources needed to develop, validate, and compare deep learning models in a standardized environment.

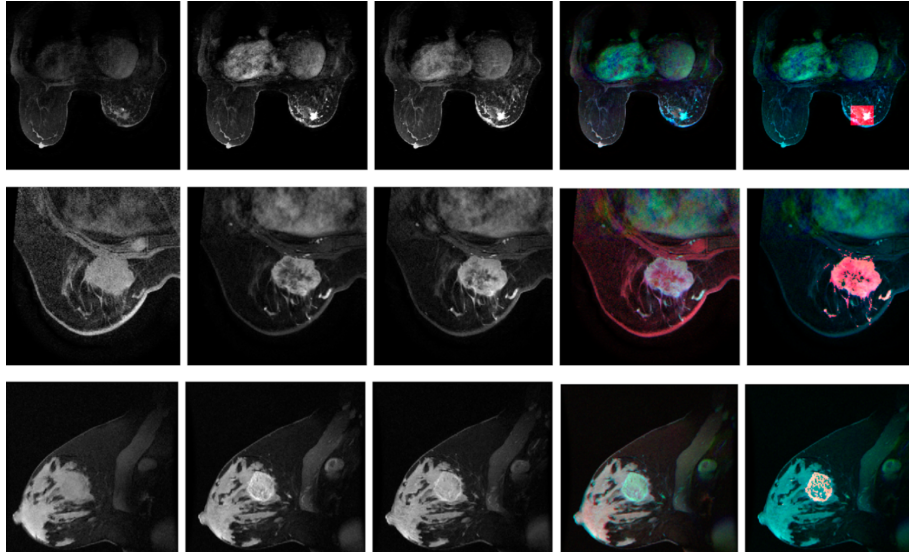


Figure 1: Dynamic Contrast-Enhanced MRI Visualization and Tumor Segmentation. Representative DCE-MRI examples from three datasets: Top row (Duke), middle row (I-SPY 1), and bottom row (I-SPY 2). Each row shows pre-contrast, early post-contrast, and late post-contrast acquisitions (left), RGB fusion of all three phases (center), and tumor segmentation overlaid in red (right). The Duke dataset example uses a bounding box for tumor localization.

2 Methods

2.1 BreastDCEDL Dataset Composition

BreastDCEDL is integrated from three datasets from The Cancer Imaging Archive (TCIA) [3]: I-SPY2 (Investigation of Serial Studies to Predict Your Therapeutic Response with Imaging And moLecular Analysis 2) dataset [13, 22], I-SPY1 (QuantumLeap Healthcare Collaborative) trial dataset [9, 20] which is quite similar to the I-SPY-2 dataset, and Duke [1] dataset. I-SPY2 contains 985 patients, 3 had missing clinical data. In I-SPY-1, several cases have missing DCE-MRI data, with only 172 patients having at least 3 scans. Duke contains 922, from which 6 had missing DCE data. This integration created a cohort of 2,070 patients (Table 1).

Table 1: Patient demographic characteristics and biomarker statuses in the BreastDCEDL database

Section	Characteristic	DUKE	I-SPY1	I-SPY2	Overall
Demographics	Age (mean \pm SD)	52.4 \pm 11.2	48.0 \pm 8.9	48.8 \pm 10.5	50.3 \pm 10.5
	Race: Black	200 (21.8%)	28 (16.3%)	117 (11.9%)	345 (16.3%)
	Race: White	648 (70.7%)	123 (71.5%)	785 (79.9%)	1556 (75.0%)
	Total patients	916 (100.0%)	172 (100.0%)	982 (100.0%)	2070 (100.0%)
HR status	HR+	696 (76.0%)	95 (55.9%)	536 (54.6%)	1327 (64.3%)
	HR-	220 (24.0%)	75 (44.1%)	446 (45.4%)	741 (35.7%)
Receptor subtype	HER2+	163 (17.8%)	53 (30.8%)	242 (24.6%)	458 (22.1%)
	HR+/HER2-	592 (64.6%)	66 (38.4%)	381 (38.8%)	1039 (50.2%)
	Triple Negative	161 (17.6%)	43 (25.0%)	359 (36.6%)	563 (27.7%)
pCR	pCR+	63 (21.1%)	49 (28.5%)	316 (32.2%)	428 (20.6%)
	pCR-	235 (78.9%)	123 (71.5%)	666 (67.8%)	1024 (49.4%)

Notes: HR = Hormone Receptor (includes ER and/or PR positive status); HER2+ = HER2 positive regardless of HR status; HR+/HER2- = Hormone receptor positive and HER2 negative; Triple Negative = ER-/PR-/HER2-; pCR = pathological Complete Response. Percentages for pCR are calculated based on patients with available pCR data (DUKE: 298 patients, I-SPY1: 172 patients, I-SPY2: 982 patients, Overall: 1452 patients).

2.2 DCE-MRI Data Standardization

The raw data from I-SPY2, I-SPY1, and Duke datasets were collected from multiple centers, with I-SPY2 alone contributing data from more than 22 centers. We extracted slice location and acquisition time from DICOM metadata, organized data temporally by acquisition time and spatially along anatomical axes. The various datasets stored information such as modality type, contrast injection time, scan intervals across different DICOM tags with diverse filename formats and metadata descriptions, requiring systematic reconciliation.

While the original DICOM data format used 16-bit integer or 16-bit unsigned integer representation, we preserved the full dynamic range by converting to 64-bit floating point format during standardization. We organized the 3D files with a clear naming convention following the pattern `<dataset>_<patient id>.acq<acquisition number>`. To facilitate validation and further exploration of the MRI data, we provided a mapping table linking the raw DICOM slices to the 3D NIFTI planes in the project’s Git repository, along with a comprehensive DICOM tag dictionary.

2.3 Tumor Annotation Processing and Integration

In addition to raw MRI slices, the I-SPY trial databases contain processed data and information on tumor segmentation, ROI delineation, selected SER images (precontrast, early postcontrast and late postcontrast), enhancement calculation maps, and analysis masks that encode the segmentation process. We converted these analysis masks into binary 3D files where tumor regions were coded as 1 and background tissue as 0. The masks were oriented along the same axis as the original MRI scans to facilitate precise alignment.

For the Duke dataset, annotations were created based on the precontrast DCE-MR images, the first postcontrast images, and the difference between the two. Expert radiologists annotated bounding boxes on planes containing the largest tumor area. We transformed these bounding box coordinates to correspond with our standardized DCE-MRI alignment. It is important to note that while MRI scans across all datasets can contain multiple tumors (up to 9 tumors per scan in the Duke dataset), only the largest (primary) tumor was annotated in each case.

2.4 Clinicopathologic Data and Tumor Characteristics Harmonization

We standardized heterogeneous clinical metadata across the three source datasets, unifying common demographic features (age at diagnosis, race, menopausal status) and tumor characteristics (HR and HER2 status). HR status determination varied by institutional thresholds: I-SPY2 used $\geq 1\%$ staining (most sensitive), Duke employed Allred score > 3 (intermediate), and I-SPY1 applied $\geq 10\%$ staining (most stringent). Consequently, I-SPY2 classified the greatest proportion of tumors as HR+, while I-SPY1 classified the fewest. For HER2 status, Duke used a FISH ratio > 2.2 , while both I-SPY trials used ≥ 2.0 , resulting in marginally fewer tumors classified as HER2+ in the Duke dataset. We calculated tumor volumes for I-SPY datasets by multiplying malignant voxel counts by physical voxel dimensions, whereas the Duke dataset provided tumor volumes pre-categorized into five size classes (1–5 cm³). We excluded patients with fewer than 3 MRI acquisitions and organized all clinicopathologic and imaging data in standardized CSV format, documenting scan parameters, physical dimensions, SER timepoints, and clinical variables. Population characteristics are summarized in Table 1.

2.5 Vision Transformer Implementation for pCR Prediction

We implemented a Vision Transformer (ViT) approach for predicting pathologic complete response from DCE-MRI data. Input preparation involved generating RGB-fused images from DCE-MRI slices containing tumor regions, with pre-contrast, early post-contrast, and late post-contrast acquisitions assigned to red, green, and blue channels respectively, as illustrated in Figure 2. For I-SPY trials,

we utilized Signal Enhancement Ratio (SER) timepoints 0, 2, and the minimum between the last index and 6; for the Duke dataset, timepoints 0, 1, and the final acquisition were used. All images underwent MinMax normalization and conversion to 8-bit format for compatibility with pre-trained models.

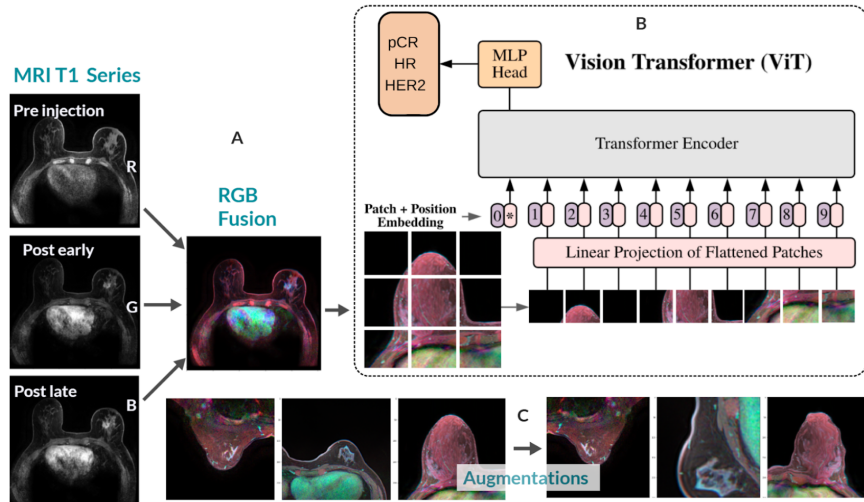


Figure 2: DCE-MRI fusion as input to a classification Vision Transformer (ViT). **A** Fusion of the images acquired at three timepoints: precontrast, early post-contrast, and late postcontrast. Each set of images is converted to one of the RGB colors, after which they are all fused into a set of 2D RGB images. **B** Scheme of a vision transformer-based model: an RGB image is cropped into patches, which are embedded as tokens, then passed to an NLP architecture such as BERT. **C** Examples of image augmentation used for model training. Panel B adapted from [5]

Our inference pipeline consisted of two stages. First, we passed each RGB-fused slice through the ViT model, and aggregated slice-level predictions (using minimum, mean, and median operations) to generate patient-level scores. Second, we combined these imaging-derived features with clinical variables (HR status, HER2 status, age, and race) using machine learning methods (Random Forest and Gradient Boosting).

To demonstrate the approach’s versatility, we performed a case study using the I-SPY2 cohort, incorporating additional clinical variables including MammaPrint scores, treatment regimens, and derived features such as tumor size and shape metrics. This methodology illustrates a recommended workflow for researchers utilizing the BreastDCEDL dataset with their own institutional data.

The implementation utilized the Hugging Face Transformers library, PyDicom for DICOM processing, and PyTorch for deep learning components, allowing efficient application of transformer architectures to breast cancer treatment

response prediction.

2.6 Standardized Benchmark Establishment

We created fixed Train-Validation-Test partitions for the BreastDCEDL dataset to ensure reproducible benchmarking across studies. We randomly split patients with available pathological complete response status according to response rate, and distributed remaining patients based on HER2 status. We redistributed a few randomly selected patients between groups based on pathological complete response, HR and HER2 status to maintain balanced biomarker representation across all dataset partitions, as much as possible.

The final dataset partitions comprised 1,099 patients (29.3% pCR rate) for training, 177 patients (29.9% pCR rate) for validation, and 176 patients (30.1% pCR rate) for testing, with an overall pCR rate of 29.5% across all 1,452 patients with available pCR data. These standardized splits are provided with the data set to facilitate the direct comparison of different modeling approaches and ensure reproducible research results.

3 Results

3.1 BreastDCEDL: A Standardized Deep Learning-Ready DCE-MRI Dataset

We developed BreastDCEDL, the first comprehensive, standardized DCE-MRI dataset designed specifically for deep learning applications and computational analysis including radiomics. The dataset consolidates data from three major clinical cohorts—Duke (n=916), I-SPY1 (n=172), and I-SPY2 (n=982)—creating an unprecedented resource of 2,070 patients with preserved original DICOM intensity values, spatial resolution, and imaging parameters. All data have been converted to standardized 3D NIfTI format with complete clinical annotations and ready-to-use train/validation/test partitions. The data organization structure and representative examples from each cohort are presented in Figure 3.

3.2 Standardized Benchmark Partitions

Our standardized benchmark partitions maintain consistent pCR rates across Train-Validation-Test splits (29.3%, 29.9%, and 30.1% respectively) among the 1,452 patients with available response data. This design enables fair and reproducible comparisons between computational methods while preserving the clinical heterogeneity essential for robust model development.

3.3 Vision Transformer Performance and Comparison with Prior Studies

Our ViT implementation demonstrated strong performance in predicting pathologic complete response, achieving results that compare favorably with previ-

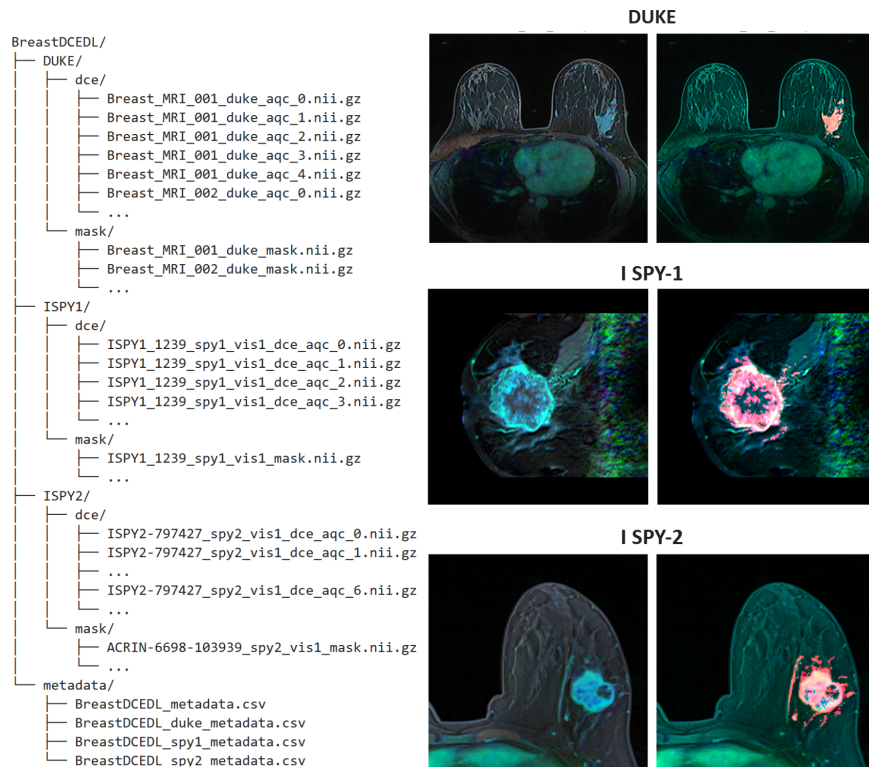


Figure 3: BreastDCEDL dataset organization and representative examples. Data organization structure showing standardized 3D NIFTI format with clinical annotations, and representative DCE-MRI examples from each contributing cohort demonstrating the diversity of imaging characteristics across institutions.

ous studies (Table 2). The model performed particularly well on the I-SPY2 dataset, achieving an AUC of 0.85 overall and 0.94 for HR+/HER2⁻ tumors with 93% accuracy and perfect precision. This performance exceeds that of Li et al. [13], who reported an AUC of 0.83 using traditional machine learning on DCE-MRI features from 384 I-SPY2 patients, and aligns with Dammu et al. [4], who achieved an AUC of 0.70 using RGB fusion with Residual CNN on 155 I-SPY1 patients, while our model achieved 0.68 AUC on 172 unfiltered I-SPY1 patients. Our results also substantially improve upon the recent large-scale study by Li et al. [14], who analyzed 814 I-SPY2 patients and achieved AUC values ranging from 0.68 to 0.74 across receptor subtypes, with HR+/HER2⁻ showing the highest performance—consistent with our findings.

Table 2: Pathological complete response prediction results

Receptor Status	N	pCR Rate	Accuracy	AUC	Sensitivity	Specificity	Precision	NPV
Overall Test Set Performance								
Overall	177	30.1%	0.75	0.72	0.27	0.95	0.70	0.75
HR ⁻ /HER2 ⁻	63	36.5%	0.65	0.63	0.26	0.88	0.55	0.67
HER2+	43	42.0%	0.72	0.68	0.44	0.92	0.80	0.70
HR+/HER2 ⁻	69	16.0%	0.86	0.64	0.10	1.00	1.00	0.86
Performance by Dataset								
I-SPY1	35	34.3%	0.72	0.68	0.17	1.00	1.00	0.70
I-SPY2	99	32.3%	0.73	0.78	0.28	0.94	0.70	0.73
Duke	43	21.0%	0.77	0.54	0.22	0.91	0.40	0.82
I-SPY2 with clinical, demographic and tumor features								
Overall I-SPY2	99	32.3%	0.76	0.85	0.34	0.96	0.79	0.75
HR ⁻ /HER2 ⁻	40	47.5%	0.68	0.75	0.32	1.00	1.00	0.62
HER2+	19	42.1%	0.78	0.84	0.75	0.82	0.75	0.82
HR+/HER2 ⁻	40	12.5%	0.93	0.94	0.41	1.00	1.00	0.92

Notes: pCR = pathological complete response; NPV = negative predictive value; HR = Hormone Receptor (ER and/or PR positive); HER2+ = HER2 positive regardless of HR status; HR+/HER2⁻ = Hormone receptor positive and HER2 negative; Triple Negative = ER⁻/PR⁻/HER2⁻.

For HER2+ tumors, our model achieved an AUC of 0.68 overall on Breast-DCE-MRI and 0.84 on the I-SPY2 cohort, which is comparable to Mohamed et al. [18], who reported AUCs of 0.77 and 0.85 on small validation cohorts (n=28 and n=20) using pre-trained CNN with SVM approaches. Performance for triple-negative tumors remained challenging but competitive, with our overall AUC of 0.63 and I-SPY2 AUC of 0.75, aligning with current literature standards where Li et al. [14] achieved less than 0.63 AUC on a single-center cohort of 163 triple-negative cases.

Several studies have incorporated additional MRI sequences beyond DCE-MRI to enhance predictive performance. Liu et al. [17] achieved an AUC of 0.86 for HR+/HER2⁻ tumors using machine learning on features extracted from DCE-MRI, T2-weighted imaging, and diffusion-weighted imaging across 586 patients from four hospitals. Similarly, Janssen et al. [10] utilized T2-

weighted and T1-weighted sequences alongside DCE-MRI, achieving an AUC of 0.86 on a private single-center dataset of 61 patients. While these multimodal approaches demonstrate the potential value of incorporating diverse imaging information, our DCE-MRI-only method achieved comparable performance using a single imaging modality, suggesting that transformer architectures can effectively capture the complex spatiotemporal patterns inherent in dynamic contrast-enhanced sequences. This indicates that substantial improvements may be achievable when additional modalities are incorporated into BreastDCEDL.

Feature importance analysis revealed that tumor volume consistently ranked as the most critical predictor across all tested models, with tumor volume, bounding box volume, and deep learning-derived features appearing at the top of importance rankings (Figure 4). Age typically ranked high in predictive importance, followed by hormone receptor status, while race consistently ranked lowest among clinical variables. These findings underscore the complementary value of quantitative imaging biomarkers and clinical parameters in treatment response prediction.

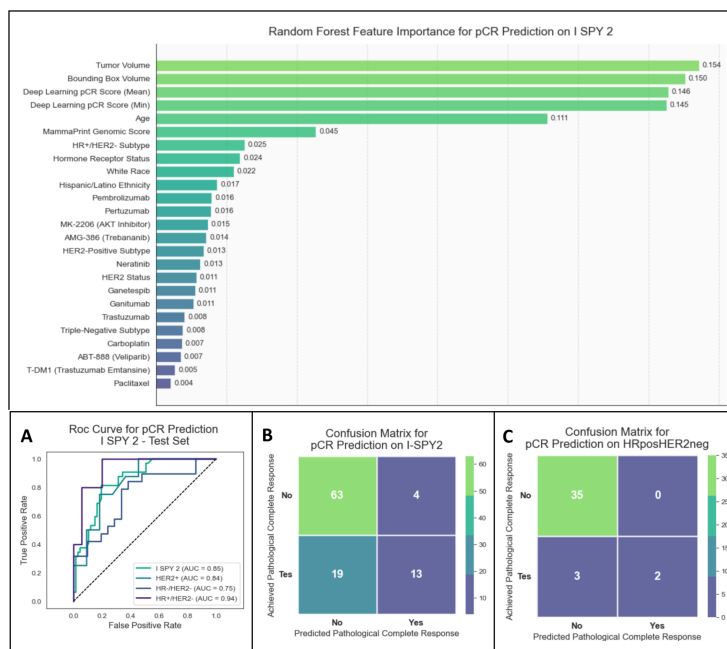


Figure 4: Random Forest model performance for pathological complete response (pCR) prediction in the I-SPY2 cohort. Top panel shows feature importance rankings for pCR prediction. Bottom panels show: **A** Receiver operating characteristic (ROC) curves for overall cohort and hormone receptor subtypes, **B** Confusion matrix showing model classification performance on I-SPY2, and **C** Confusion matrix showing model classification performance on HR+/HER2- subtype of I-SPY2 cohort.

4 Discussion and Conclusion

We have presented BreastDCEDL, the first comprehensive, standardized, and publicly available DCE-MRI dataset for breast cancer, comprising 2,070 patients across three major cohorts. This resource addresses critical barriers that have long impeded progress in applying advanced deep learning methods to breast cancer imaging. Critically, BreastDCEDL preserves original DICOM acquisition parameters without imposed preprocessing, providing comprehensive metadata including spatial resolutions, slice thicknesses, and scanner specifications. This approach enables researchers to develop and evaluate their own normalization and harmonization methods—a fundamental requirement for advancing MRI research methodology.

Our Vision Transformer model achieved competitive performance with published benchmarks, demonstrating robust discriminative capacity. Across 177 test cases, the model attained 75% accuracy and 0.72 AUC (Table 2). The model exhibited high specificity (0.95) with corresponding low sensitivity (0.27), reflecting a conservative prediction profile that minimizes false positives. This performance characteristic aligns with clinical priorities, where accurate identification of non-responders provides critical pre-treatment guidance, while false positives carry lower clinical risk given that patients proceed to neoadjuvant chemotherapy regardless. For HR+/HER2⁻ tumors in the I-SPY2 cohort with integrated clinical data (N=40, 12.5% pCR rate), our approach achieved exceptional performance (AUC 0.94, accuracy 93%, NPV 92%), representing state-of-the-art results that could inform treatment decisions.

Several limitations warrant consideration. We observed considerable performance variations across datasets (I-SPY2: AUC 0.78; Duke: AUC 0.54; I-SPY1: AUC 0.68), likely reflecting I-SPY2’s larger sample size, superior image quality, and larger tumor volumes. Additional factors include imaging protocol diversity and our preservation of raw, unprocessed data—while methodologically valuable for harmonization research, this approach may reduce performance consistency compared to normalized datasets. Our methodological choices impose several constraints. The 8-bit representation and RGB fusion approach, while enabling pre-trained model leverage, potentially obscures DCE-MRI’s full spatiotemporal patterns. The RGB fusion method blurs specific enhancement patterns from individual timepoints that may be critical for biomarker prediction. Furthermore, our 2D implementation fails to capture the complete 3D spatiotemporal information inherent in DCE-MRI sequences, representing a significant limitation for comprehensive tumor characterization.

The Vision Transformer architecture presents additional constraints. Fixed non-overlapping patches, while suitable for natural images, limit analysis of fine-grained medical imaging details. Future implementations could benefit from architectures like Shifted Window Transformers [16], that better handle medical imaging’s spatial granularity requirements. Additionally, our two-stage approach—combining deep learning features with clinical variables through traditional machine learning—while practical for feature impact assessment, could be superseded by end-to-end transformer architectures directly incorporating

clinical data within the deep learning framework.

Transformer models offer more than just powerful representation learning; they generate attention maps that may provide intriguing insights into DCE-MRI interpretation. These attention patterns could potentially identify novel imaging biomarkers in breast MRI, improving our understanding of treatment response prediction. By making BreastDCEDL publicly available alongside code and pre-trained models, we aim to accelerate progress in AI-assisted breast cancer care and enable more advanced architectural innovations to address current limitations.

5 Data and Code Availability

Code for data processing and model implementation is available at GitHub: <https://github.com/naomifridman/BreastDCEDL>. Processed datasets including the I-SPY1 subset, tumor-centered Duke cohort samples, and pre-trained model weights are deposited on Zenodo [6] (<https://doi.org/10.5281/zenodo.15627233>). Complete imaging datasets from I-SPY1, I-SPY2, and Duke cohorts can be accessed through The Cancer Imaging Archive (TCIA) and converted to standardized NIFTI format using our provided processing pipeline. Standardized train-validation-test splits and comprehensive metadata are included to ensure reproducible model development and evaluation.

References

- [1] S. Ashirbani. Dynamic contrast-enhanced magnetic resonance images of breast cancer patients with tumor locations (duke-breast-cancer-mri) - the cancer imaging archive (tcia) public access - cancer imaging archive wiki, 2021. URL <https://wiki.cancerimagingarchive.net/pages/viewpage.action?pageId=70226903>.
- [2] N. Braman, M. E. Adoui, M. Vulchi, P. Turk, M. Etesami, P. Fu, K. Bera, S. Drisis, V. Varadan, D. Plecha, M. Benjelloun, J. Abraham, and A. Madabhushi. Deep learning-based prediction of response to her2-targeted neoadjuvant chemotherapy from pre-treatment dynamic breast mri: A multi-institutional validation study. *arXiv*, 2020. doi: 10.48550/arxiv.2001.08570.
- [3] K. Clark, B. Vendt, K. Smith, J. Freymann, J. Kirby, P. Koppel, S. Moore, S. Phillips, D. Maffitt, M. Pringle, L. Tarbox, and F. Prior. The cancer imaging archive (tcia): Maintaining and operating a public information repository. *Journal of Digital Imaging*, 26(6):1045–1057, 2013. ISSN 0897-1889. doi: 10.1007/s10278-013-9622-7.
- [4] Hongyi Dammu, Thomas Ren, and Tim Q. Duong. Deep learning prediction of pathological complete response, residual cancer burden, and progression-

- free survival in breast cancer patients. *PLOS ONE*, 18(1):e0280148, 2023. doi: 10.1371/journal.pone.0280148.
- [5] Alexey Dosovitskiy, Lucas Beyer, Alexander Kolesnikov, Dirk Weissenborn, Xiaohua Zhai, Thomas Unterthiner, Mostafa Dehghani, Matthias Minderer, Georg Heigold, Sylvain Gelly, Jakob Uszkoreit, and Neil Houlsby. An image is worth 16x16 words: Transformers for image recognition at scale. *arXiv*, 2020. doi: 10.48550/arxiv.2010.11929.
- [6] Naomi Fridman, Bubby Solway, Tomer Fridman, and Itamar Barnea. Breastdcedl: A deep learning-ready breast dce-mri dataset. 2025. doi: 10.5281/zenodo.15627233. URL <https://zenodo.org/records/15627233>.
- [7] Roberto Lo Gullo, Sarah Eskreis-Winkler, Elizabeth A. Morris, and Katja Pinker. Machine learning with multiparametric magnetic resonance imaging of the breast for early prediction of response to neoadjuvant chemotherapy. *The Breast : official journal of the European Society of Mastology*, 49: 115–122, 2019. ISSN 0960-9776. doi: 10.1016/j.breast.2019.11.009.
- [8] Essam H. Houssein, Marwa M. Emam, Abdelmgeid A. Ali, and Pon-nuthurai Nagarathnam Suganthan. Deep and machine learning techniques for medical imaging-based breast cancer: A comprehensive review. *Expert Systems with Applications*, 167:114161, 2021. ISSN 0957-4174. doi: 10.1016/j.eswa.2020.114161.
- [9] Nola M. Hylton, Constantine A. Gatsonis, Mark A. Rosen, Constance D. Lehman, David C. Newitt, Savannah C. Partridge, Wanda K. Bernreuter, Etta D. Pisano, Elizabeth A. Morris, Paul T. Weatherall, Sandra M. Polin, Gillian M. Newstead, Helga S. Marques, Laura J. Esserman, Mitchell D. Schnall, and For the ACRIN 6657 Trial Team and I-SPY 1 TRIAL Investigators. Neoadjuvant chemotherapy for breast cancer: Functional tumor volume by mr imaging predicts recurrence-free survival—results from the acrin 6657/calgb 150007 i-spy 1 trial. *Radiology*, 279(1):44–55, 2015. ISSN 0033-8419. doi: 10.1148/radiol.2015150013.
- [10] L. M. Janssen, M. H. A. Janse, Vries, B. B. L. Penning de, Velden, B. H. M. van der, Ben, E. J. M. Wolters-van der, Bosch, S. M. van den, A. Sartori, C. Jovelet, M. J. Agterof, Huinink, D. Ten Bokkel, E. W. Bouman-Wammes, Diest, P. J. van, Wall, E. van der, S. G. Elias, and K. G. A. Gilhuijs. Predicting response to neoadjuvant chemotherapy with liquid biopsies and multiparametric mri in patients with breast cancer. *npj Breast Cancer*, 10(1):10, 2024. ISSN 2374-4677. doi: 10.1038/s41523-024-00611-z.
- [11] Sunghoon Joo, Eun Sook Ko, Soonhwan Kwon, Eunjoo Jeon, Hyungsik Jung, Ji-Yeon Kim, Myung Jin Chung, and Young-Hyuck Im. Multimodal deep learning models for the prediction of pathologic response to neoadjuvant chemotherapy in breast cancer. *Scientific Reports*, 11(1):18800, 2021. doi: 10.1038/s41598-021-98408-8.

- [12] Jun Li, Junyu Chen, Yucheng Tang, Ce Wang, Bennett A. Landman, and S. Kevin Zhou. Transforming medical imaging with transformers? a comparative review of key properties, current progresses, and future perspectives. *Medical Image Analysis*, 85:102762, 2023. ISSN 1361-8415. doi: 10.1016/j.media.2023.102762.
- [13] Wen Li, David C. Newitt, Jessica Gibbs, Lisa J. Wilmes, Ella F. Jones, Vignesh A. Arasu, Fredrik Strand, Natsuko Onishi, Alex Anh-Tu Nguyen, John Kornak, Bonnie N. Joe, Elissa R. Price, Haydee Ojeda-Fournier, Mohammad Eghtedari, Katrina W. Zamora, Stefanie A. Woodard, Heidi Umphrey, Wanda Bernreuter, Michael Nelson, An Ly Church, Patrick Bolan, Theresa Kuritza, Kathleen Ward, Kevin Morley, Dulcy Wolverton, Kelly Fountain, Dan Lopez-Paniagua, Lara Hardesty, Kathy Brandt, Elizabeth S. McDonald, Mark Rosen, Despina Kontos, Hiroyuki Abe, Deepa Sheth, Erin P. Crane, Charlotte Dillis, Pulin Sheth, Linda Hovanessian-Larsen, Dae Hee Bang, Bruce Porter, Karen Y. Oh, Neda Jafarian, Alina Tudorica, Bethany L. Niell, Jennifer Drukteinis, Mary S. Newell, Michael A. Cohen, Marina Giurescu, Elise Berman, Constance Lehman, Savannah C. Partridge, Kimberly A. Fitzpatrick, Marisa H. Borders, Wei T. Yang, Basak Dogan, Sally Goudreau, Thomas Chenevert, Christina Yau, Angela DeMichele, Don Berry, Laura J. Esserman, and Nola M. Hylton. Predicting breast cancer response to neoadjuvant treatment using multi-feature mri: results from the i-spy 2 trial. *NPJ Breast Cancer*, 6(1):63, 2020. ISSN 2374-4677. doi: 10.1038/s41523-020-00203-7.
- [14] Wen Li, Natsuko Onishi, Jessica E. Gibbs, Lisa J. Wilmes, Nu N. Le, Pouya Metanat, Elissa R. Price, Bonnie N. Joe, John Kornak, Christina Yau, Denise M. Wolf, Mark Jesus M. Magbanua, Barbara LeStage, Veer, Laura J. van 't, Angela M. DeMichele, Laura J. Esserman, and Nola M. Hylton. Mri-based model for personalizing neoadjuvant treatment in breast cancer. *Tomography*, 11(3):26, 2025. doi: 10.3390/tomography11030026.
- [15] Michael Z. Liu, Simukayi Mutasa, Peter Chang, Maham Siddique, Sachin Jambawalikar, and Richard Ha. A novel cnn algorithm for pathological complete response prediction using an i-spy trial breast mri database. *Magnetic Resonance Imaging*, 73:148–151, 2020. ISSN 0730-725X. doi: 10.1016/j.mri.2020.08.021.
- [16] Ze Liu, Yutong Lin, Yue Cao, Han Hu, Yixuan Wei, Zheng Zhang, Stephen Lin, and Baining Guo. Swin transformer: Hierarchical vision transformer using shifted windows. *arXiv*, 2021. doi: 10.48550/arxiv.2103.14030.
- [17] Zhenyu Liu, Zhuolin Li, Jinrong Qu, Renzhi Zhang, Xuezhi Zhou, Longfei Li, Kai Sun, Zhenchao Tang, Hui Jiang, Hailiang Li, Qianqian Xiong, Yingying Ding, Xinming Zhao, Kun Wang, Zaiyi Liu, and Jie Tian. Radiomics of multiparametric mri for pretreatment prediction of pathologic

- complete response to neoadjuvant chemotherapy in breast cancer: A multicenter study. *Clinical Cancer Research*, 25(12):3538–3547, 2019. ISSN 1078-0432. doi: 10.1158/1078-0432.ccr-18-3190.
- [18] Rania M. Mohamed, Bikash Panthi, Beatriz E. Adrada, Medine Boge, Rosalind P. Candelaria, Huiqin Chen, Mary S. Guirguis, Kelly K. Hunt, Lei Huo, Ken-Pin Hwang, Anil Korkut, Jennifer K. Litton, Tanya W. Moseley, Sanaz Pashapoor, Miral M. Patel, Brandy Reed, Marion E. Scoggins, Jong Bum Son, Alastair Thompson, Debu Tripathy, Vicente Valero, Peng Wei, Jason White, Gary J. Whitman, Zhan Xu, Wei Yang, Clinton Yam, Jingfei Ma, and Gaiane M. Rauch. Multiparametric mri-based radiomic models for early prediction of response to neoadjuvant systemic therapy in triple-negative breast cancer. *Scientific Reports*, 14(1):16073, 2024. doi: 10.1038/s41598-024-66220-9.
- [19] David Newitt and Nola Hylton. Dataset - breast-mri-nact-pilot. *The Cancer Imaging Archive*, 2016. doi: 10.7937/k9/tcia.2016.qhsyhjky. URL <https://wiki.cancerimagingarchive.net/display/Public/Breast-MRI-NACT-Pilot#22513764fb2b62ab82ef47da8b39106de8b728bd>.
- [20] David Newitt, Nola Hylton, and Archive., on behalf of the I-SPY 1 Network and ACRIN 6657 Trial Team. Ispy1 - the cancer imaging archive (tcia). URL <https://www.cancerimagingarchive.net/collection/ispy1/>.
- [21] Ashish Vaswani, Noam Shazeer, Niki Parmar, Jakob Uszkoreit, Llion Jones, Aidan N Gomez, Lukasz Kaiser, and Illia Polosukhin. Attention is all you need. *arXiv*, 2017. doi: 10.48550/arxiv.1706.03762.
- [22] Haiyun Wang and Douglas Yee. I-spy 2: a neoadjuvant adaptive clinical trial designed to improve outcomes in high-risk breast cancer. *Current Breast Cancer Reports*, 11(4):303–310, 2019. ISSN 1943-4588. doi: 10.1007/s12609-019-00334-2.
- [23] Wei Wei, Menghang Ma, and Zhenyu Liu. Research progress of artificial intelligence in evaluating the efficacy of neoadjuvant chemotherapy for breast cancer. *EngMedicine*, 1(2):100024, 2024. ISSN 2950-4899. doi: 10.1016/j.engmed.2024.100024.